AGU PUBLICATIONS

JGR

Journal of Geophysical Research: Space Physics

COMMENT

10.1002/2016JA022662

This article is a comment on *Martinis et al.* [2015] doi:10.1002/2015JA021555.

**Key Points:**
- The source of OI 630.0 nm emission depletions over Mexico on 1 June 2013 was investigated
- The emission depletions were interpreted to be equatorial plasma bubbles, but this interpretation is challenged by a few uncertainties
- The characteristics of the emission depletions could be explained with MSTIDs observed over the United States on that night

**Correspondence to:**
H. Kil,
hyosub.kil@jhuapl.edu

**Citation:**
Kil, H., E. S. Miller, G. Jee, Y.-S. Kwak, Y. Zhang, and M. Nishioka (2016), Comment on "The night when the auroral and equatorial ionospheres converged" by Martinis, C., J. Baumgardner, M. Mendillo, J. Wroten, A. Coster, and L. Paxton, *J. Geophys. Res. Space Physics*, *121*, 10,599–10,607, doi:10.1002/2016JA022662.

Received 4 MAR 2016
Accepted 7 AUG 2016
Accepted article online 19 SEP 2016
Published online 24 OCT 2016



# Comment on "The night when the auroral and equatorial ionospheres converged" by Martinis, C., J. Baumgardner, M. Mendillo, J. Wroten, A. Coster, and L. Paxton

**Hyosub Kil[1], Ethan S. Miller[1], Geonhwa Jee[2], Young-Sil Kwak[3], Yongliang Zhang[1], and Michi Nishioka[4]**

[1]Johns Hopkins University Applied Physics Laboratory, Laurel, Maryland, USA, [2]Korea Polar Research Institute, Incheon, South Korea, [3]Korea Astronomy and Space Science Institute, Daejeon, South Korea, [4]National Institute of Information and Communications Technology, Tokyo, Japan

**Abstract** Intense OI 630.0 nm emission depletions were detected over Mexico by an all-sky imager during the main phase of the geomagnetic storm on 1 June 2013 (minimum *Dst* index: −119 nT). Those emission depletions were interpreted to be associated with equatorial plasma bubbles. If bubbles were responsible for those middle-latitude emission depletions, they would have been extreme bubbles which extended over 40° magnetic latitudes and 7000 km in altitude at the magnetic equator. However, a few factors challenge this interpretation. First, the emission depletions detected over Mexico showed westward drift, whereas the equatorial ionosphere including bubbles drifted eastward on that night. Second, the middle-latitude emission depletions were tilted westward with respect to the geographic meridian, but the westward tilt of bubbles was not identified. Third, the growth of bubbles was not evident when the middle-latitude emission depletions grew. The westward tilt and westward propagation of the middle-latitude emission depletions are consistent with the characteristics of medium-scale traveling ionospheric disturbances (MSTIDs) observed over the United States on that night. Thus, the emission depletions over Mexico can be interpreted to be the signature of MSTIDs.

## 1. Introduction

Plasma bubbles and medium-scale traveling ionospheric disturbances (MSTIDs) are the representative ionospheric disturbances in the low- and middle-latitude *F* regions, respectively. Plasma bubbles indicate plasma depletions relative to ambient plasma. They develop in the bottomside of the *F* region after sunset by the action of the generalized Rayleigh-Taylor instability and grow to higher altitudes and latitudes as time progresses [*Kelley*, 1989]. In optical observations, bubbles appear to be emission depletion bands elongated in the north-south direction because of the plasma depletion in the whole magnetic flux tube [e.g., *Kil et al*., 2004; *Makela and Miller*, 2008; *Martinis and Mendillo*, 2007]. Owing to the differential eastward motion of plasma in different magnetic flux tubes, the three-dimensional structure of a bubble is described by a plasma depletion shell [*Huba et al*., 2008; *Kil et al*., 2009]. Medium-scale traveling ionospheric disturbances (MSTIDs) represent wave-like ionospheric perturbations of the horizontal wavelengths of several hundred kilometers [e.g., *Otsuka et al*., 2004]. The creation of MSTIDs is understood in association with atmospheric gravity waves induced by many sources including tropospheric turbulence and auroral activity [*Fritts and Alexander*, 2003; *Hunsucker*, 1982; *Vadas and Liu*, 2009]. MSTIDs have periods of a few tens of minutes to a few hours and phase velocities of a few hundred meters per second [*Hunsucker*, 1982]. Nighttime MSTIDs in the Northern Hemisphere often show an alignment of the wavefront in the northwest-southeast direction and southwestward propagation [e.g., *Shiokawa et al*., 2003; *Tsugawa et al*., 2007]. However, deviations are also observed [*Shiokawa et al*., 2008; *Vadas and Crowley*, 2010].

Intense OI 630.0 nm emission depletions were observed over Mexico on 1 June 2013 by an all-sky imager at the McDonald Observatory (30.67°N, 104.02°W, 40° magnetic latitude) in Texas [*Martinis et al*., 2015]. A moderate level of geomagnetic storm (minimum *Dst* index: –119 nT) was recorded on 1 June, and the emission depletions were detected during the main phase of the storm. The emission depletions appeared to bifurcate and extend to higher latitudes from lower latitudes as time progressed, tilted westward with respect to geographic meridian when the depletions were viewed northward, and were as intense as those produced by equatorial plasma bubbles. In addition to those optical characteristics, satellites detected bubbles in the equatorial region in the longitudes where the middle-latitude emission depletions were observed. Some of

those properties led *Martinis et al*. [2015] to the interpretation that the emission depletions observed over Mexico were produced by equatorial plasma bubbles. If the emission depletions were produced by bubbles, those bubbles were extended from the magnetic equator to beyond 40°N magnetic latitude and from a few hundred of kilometers to 7000 km in altitude at the magnetic equator. We call these bubbles "extreme bubbles" because bubbles are normally confined within ±20° magnetic latitudes [e.g., *Kil and Heelis*, 1998]. The vertical extension of bubbles to an altitude of 7000 km has not been identified by any observations in any geomagnetic conditions.

Although some characteristics of the middle-latitude emission depletions can be understood in terms of bubbles, we point out an observation gap between the emission depletions detected in middle latitudes and bubbles detected in the equatorial region. In the OI 135.6 nm radiance map derived from the observations of the Special Sensor Ultraviolet Spectrographic Imager (SSUSI) on board the Defense Meteorological Satellite Program (DMSP) F18, bubbles appeared to be elongated up to ±20° magnetic latitudes in the Eastern Pacific and North American sectors (200°–280°E). Despite the bright background intensity poleward of the equatorial region, emission depletions were absent beyond 20°N. The absence of emission depletions at intermediate latitudes (20°–30°N magnetic latitudes) may be because equatorial bubbles have not yet grown to middle latitudes when the SSUSI observations were made. The SSUSI observations were made about an hour before the appearance of the emission depletions over Mexico. While this possibility cannot be ruled out, we can also consider the situation that bubbles simply did not grow to the intermediate latitudes. For the latter case, the emission depletions in middle latitudes are interpreted as phenomena independent of equatorial bubbles.

In this paper, we validate the two possibilities by comparing the morphologies and zonal drifts of the middle-latitude emission depletions and equatorial bubbles. In addition to the validation, we investigate the association of the middle-latitude emission depletions with MSTIDs. The observation data used for this study are described in section 2. The role of bubbles and MSTIDs in the creation of the middle-latitude emission depletions is discussed in sections 3 and 4, respectively. The conclusions of this study are given in section 5.

## 2. Data Description

The OI 630.0 nm airglow observations at the McDonald Observatory were made by a Boston University all-sky imager. The details of the airglow observations are referred to *Martinis et al*. [2015]. The OI 630.0 nm emission is produced by the dissociative recombination of the oxygen ion with the molecular oxygen. Because the intensity of the OI 630.0 nm emission intensity is proportional to the number density of the oxygen ion [e.g., *Miller et al*., 2014], plasma depletions with respect to the background ionosphere appear as emission depletions in OI 630.0 nm images. We examine the morphology and propagation of the ionospheric structures in middle latitudes using the OI 630.0 nm airglow images adopted from *Martinis et al*. [2015].

SSUSI is an imaging spectrograph and provides monochromatic images at five channels in the spectral range 115 nm to 180 nm [*Paxton et al*., 2002]. We use the OI 135.6 nm channel images to locate bubbles in the equatorial region. The OI 135.6 nm emission at night is produced by the radiative recombination of oxygen ions, and therefore, plasma depletions appear as depletions in the OI 135.6 nm intensity. DMSP F18 has a Sun-synchronous circular orbit at an altitude of 840 km. The solar local time (LT) of the orbit at the equator is near 20:00 LT.

The Coupled Ion-Neutral Dynamics Investigation (CINDI) instrument [*Heelis et al*., 2009] is one of the payloads of the Communication/Navigation Outrage Forecasting System (C/NOFS) satellite and provides measurements of the concentration and velocity of ions and neutral particles. The C/NOFS satellite had low inclination (13°) and elliptical (perigee: 400 km, apogee: 850 km) orbits. The perigee and apogee decayed to 389 and 714 km, respectively, on 1 June 2013. We examine the morphology of bubbles and the zonal motion of the ionosphere using the CINDI observations.

We investigate the activity of MSTIDs in middle latitudes using the total electron content (TEC) perturbation maps in North America. The TEC perturbation for each line of sight of a Global Positioning System (GPS) satellite is obtained by detrending the vertical TEC with 1 h running average [*Tsugawa et al*., 2007]. The perturbation TEC data are provided by the National Institute of Information and Communications Technology in Japan.

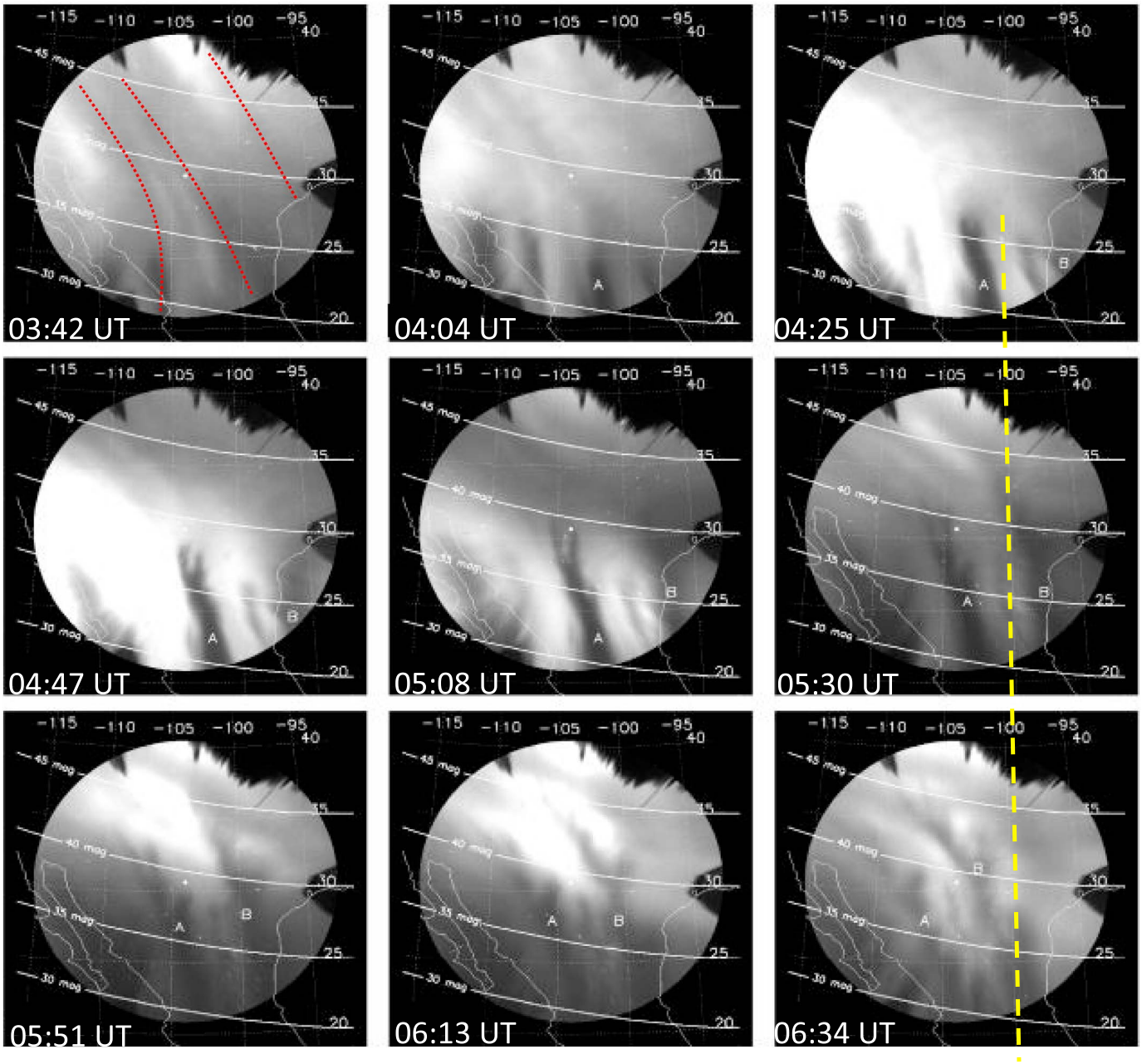


**Figure 1.** OI 630.0 nm images from 03:42 to 06:34 UT on 1 June 2013 taken by an all-sky imager at the McDonald Observatory (adopted from *Martinis et al.* [2015]). The vertical yellow line is given as a reference for the zonal movement of emission depletions. The red dotted lines in the image at 03:42 UT are given to guide weak emission depletion bands.

## 3. The Role of Equatorial Bubbles

Figure 1 shows the time series of OI 630.0 nm airglow images observed on 1 June 2013 at the McDonald Observatory (adopted from *Martinis et al.* [2015]). The emission depletion band indicated with letter "A" appears at the south of the field of view at 04:04 UT. As time progresses, the depletion appears to extend to higher latitudes. This behavior resembles the vertical and latitudinal growth of equatorial bubbles with time. In addition, the emission depletions appear to bifurcate as do equatorial bubbles [e.g., *Makela and Miller*, 2008]. Therefore, the emission depletions may be interpreted as equatorial bubbles at a glance of the airglow images. We note two things that were not pointed out by *Martinis et al.* [2015]. First, the emission depletions move westward with time. One can easily identify the westward movement of the emission depletions using the yellow vertical line as a reference. The westward drift of the emission depletions is

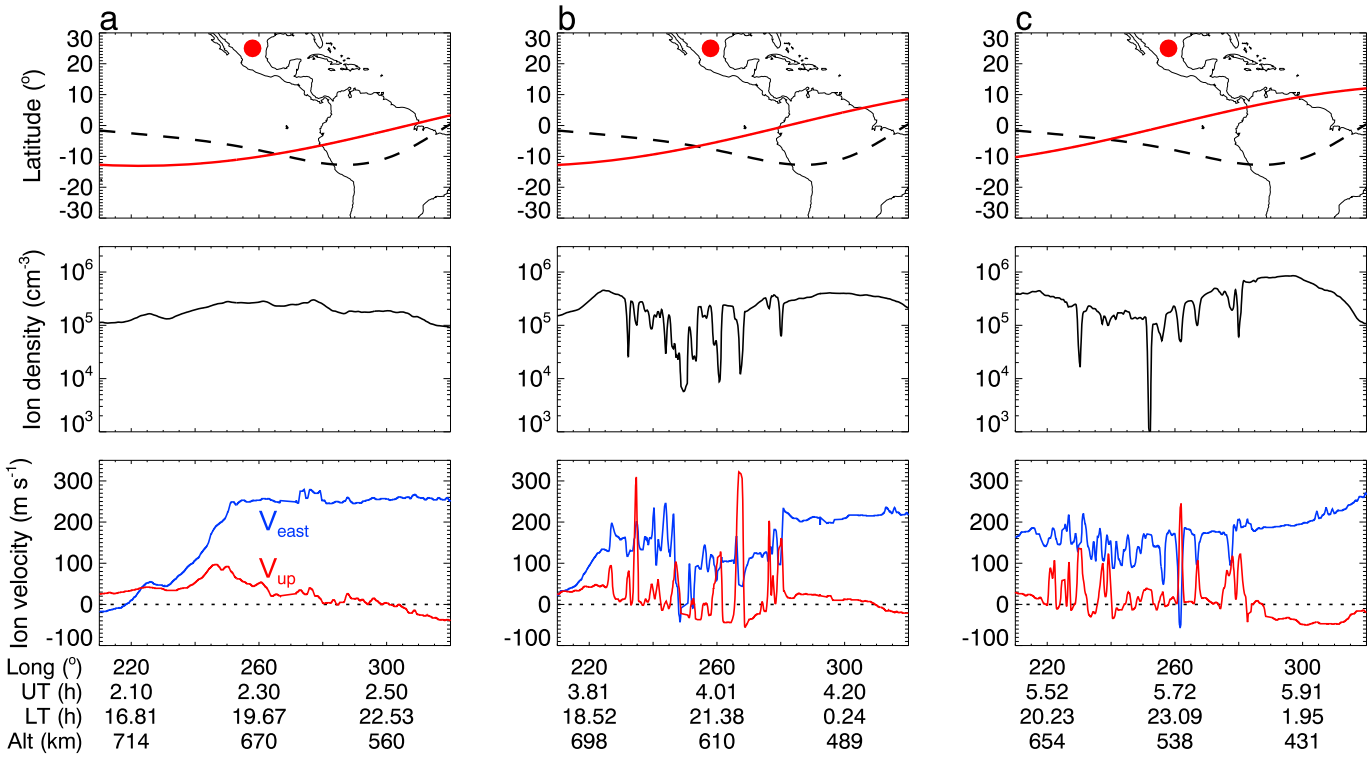


**Figure 2.** C/NOFS orbits and measurements of the ion density and velocity by CINDI around (a) 02:20, (b) 04:00, and (c) 05:40 UT on 1 June 2013. The black dashed lines in the maps indicate the geomagnetic equator. The location where the OI 630.0 nm emission depletions were detected was marked with a red dot. The zonal and meridional ion velocities in the geomagnetic coordinates are shown with blue and red lines, respectively.

inconsistent with the zonal motion of the equatorial ionosphere; typically, the ionosphere including bubbles drifts eastward at night [e.g., *Fejer et al.*, 1991; *Kil et al.*, 2014]. Although a moderate level geomagnetic storm occurred on 1 June, the zonal drift of the ionosphere on that night conformed to the typical plasma motion (see Figure 2). Second, the emission depletions are tilted westward with respect to the geographic meridian when they are viewed northward. The westward tilt of the emission depletions may be considered as the typical property of bubbles because bubbles are often tilted westward [e.g., *Martinis and Mendillo*, 2007; *Shiokawa et al.*, 2004]. However, as we show later, the westward tilt of bubbles was not obvious on that night.

The source of emission depletions at intermediate latitudes is obscure because both MSTIDs and bubbles can appear at intermediate latitudes. A critical factor for the distinction of MSTIDs from bubbles in optical images or TEC maps is their zonal motion [e.g., *Nishioka et al.*, 2009; *Miller et al.*, 2009] because typically MSTIDs appear to move westward and bubbles drift eastward at night.

Figure 2 presents the C/NOFS orbits and the measurements of the ion density and velocity by CINDI. The observations were made around (a) 02:20, (b) 04:00, and (c) 06:40 UT. The zonal motion of the background ionosphere on that night was eastward with a velocity of about 120–260 m s$^{-1}$. This observation contradicts the observation of the westward movement of the emission depletions over Mexico. From the CINDI observations, we can identify the eastward plasma motion in the magnetic latitude range of 10°S–25°N. The latitudinal mean eastward velocity is ~200 m s$^{-1}$, and the velocity does not show a decreasing tendency with latitude. Here we emphasize the uncertainty in the interpretation of the emission depletions. The emission depletions would be difficult to explain by bubbles, if the zonal velocity reversal had not happened at higher latitudes (>30°N magnetic latitude).

The eastward velocity of plasma inside bubbles is smaller than that of ambient plasma (or background). We note that the plasma motion inside bubbles represents internal turbulence. Internal turbulence is different from the motion of the envelope of bubbles [e.g., *Kil et al.*, 2014]. The envelope of a bubble is the background ionosphere. Because the zonal motion of bubbles in optical images is the motion of the envelope, the motion of emission depletions should be compared with the motion of the bubble-embedded background ionosphere.

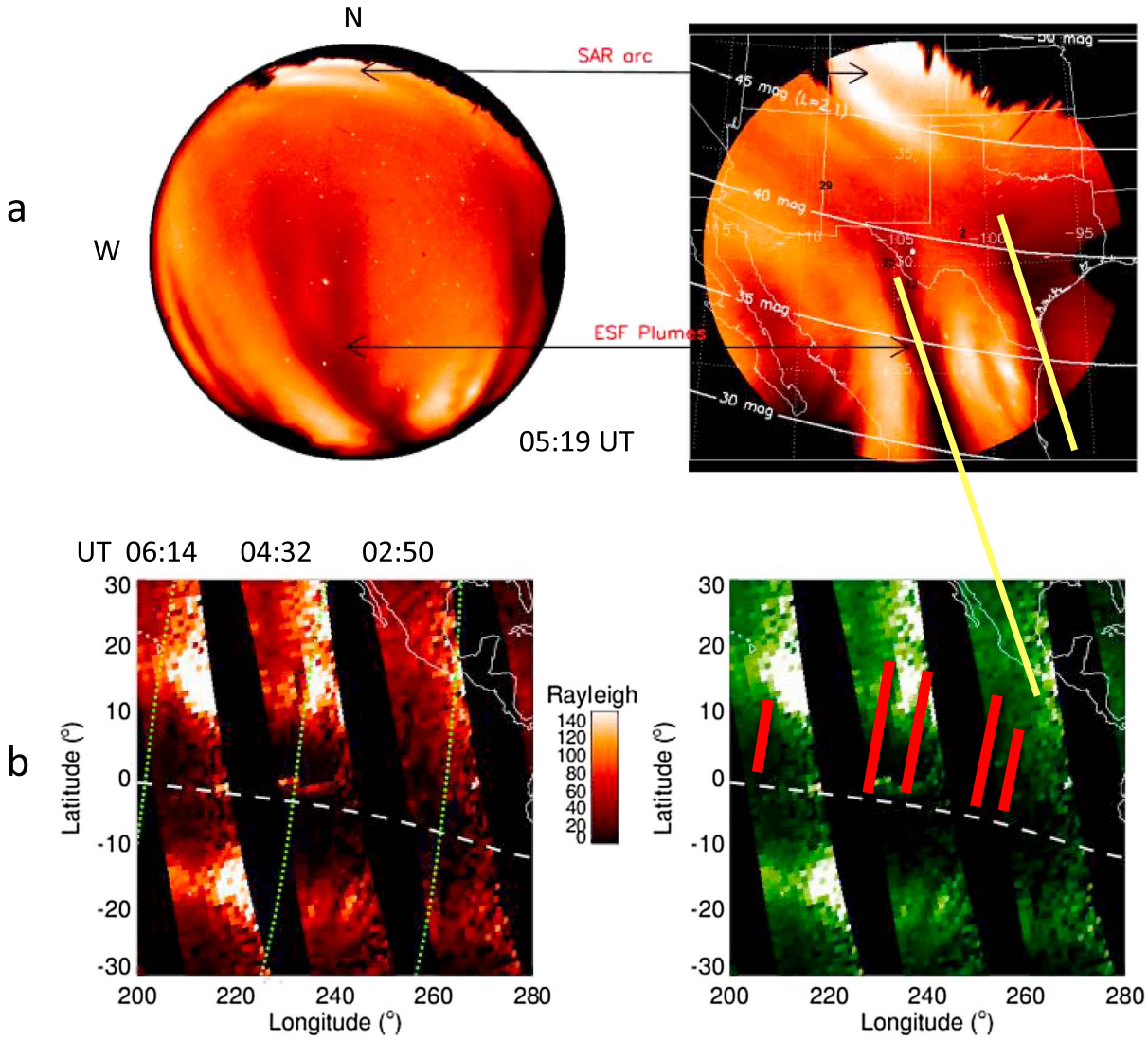


**Figure 3.** (a) OI 630.0 nm images at 05:19 UT on 1 June 2013 taken by an all-sky imager at the McDonald Observatory (adopted from *Martinis et al.* [2015]). (b) Composite SSUSI OI 135.6 nm images on the same night. The white dashed line indicates the magnetic equator and the green dots represent the geomagnetic field lines. The same SSUSI image is shown with two colors to guide the locations of bubbles. Bubbles in the equatorial region and emission depletions in middle latitudes are demarcated with red and yellow lines, respectively.

The OI 630.0 nm images at 05:19 on 1 June 2013 are shown in Figure 3a (adopted from *Martinis et al.* [2015]). The SSUSI OI 135.6 nm image is shown with two colors in Figure 3b. The magnetic equator is indicated with white dashed line and the geomagnetic field lines are shown with green dots. We can identify the emission depletion bands produced by bubbles only poleward of equatorial region because of low background intensity near the magnetic equator. The locations of some bubbles are marked with red lines in the SSUSI image with green color. As the red lines indicate, equatorial emission depletions (bubbles) are perpendicular to the magnetic equator (parallel to the geomagnetic field lines). For a comparison, the emission depletions in the all-sky image are indicated with yellow lines. The emission depletions in the all-sky image are tilted westward and the emission depletions in SSUSI image are tilted eastward with respect to the geographic meridian. Bubbles in the SSUSI image are elongated to at most 10°N in geographic latitude in the longitudes where the middle-latitude emission depletions were detected. The SSUSI observations were made at 19–20 LT and 2.5 h earlier than the all-sky image (around the longitude of 260°E). Bubbles in the SSUSI image might have grown to middle latitudes and tilted westward at later hours. However, we do not know whether these had happened.

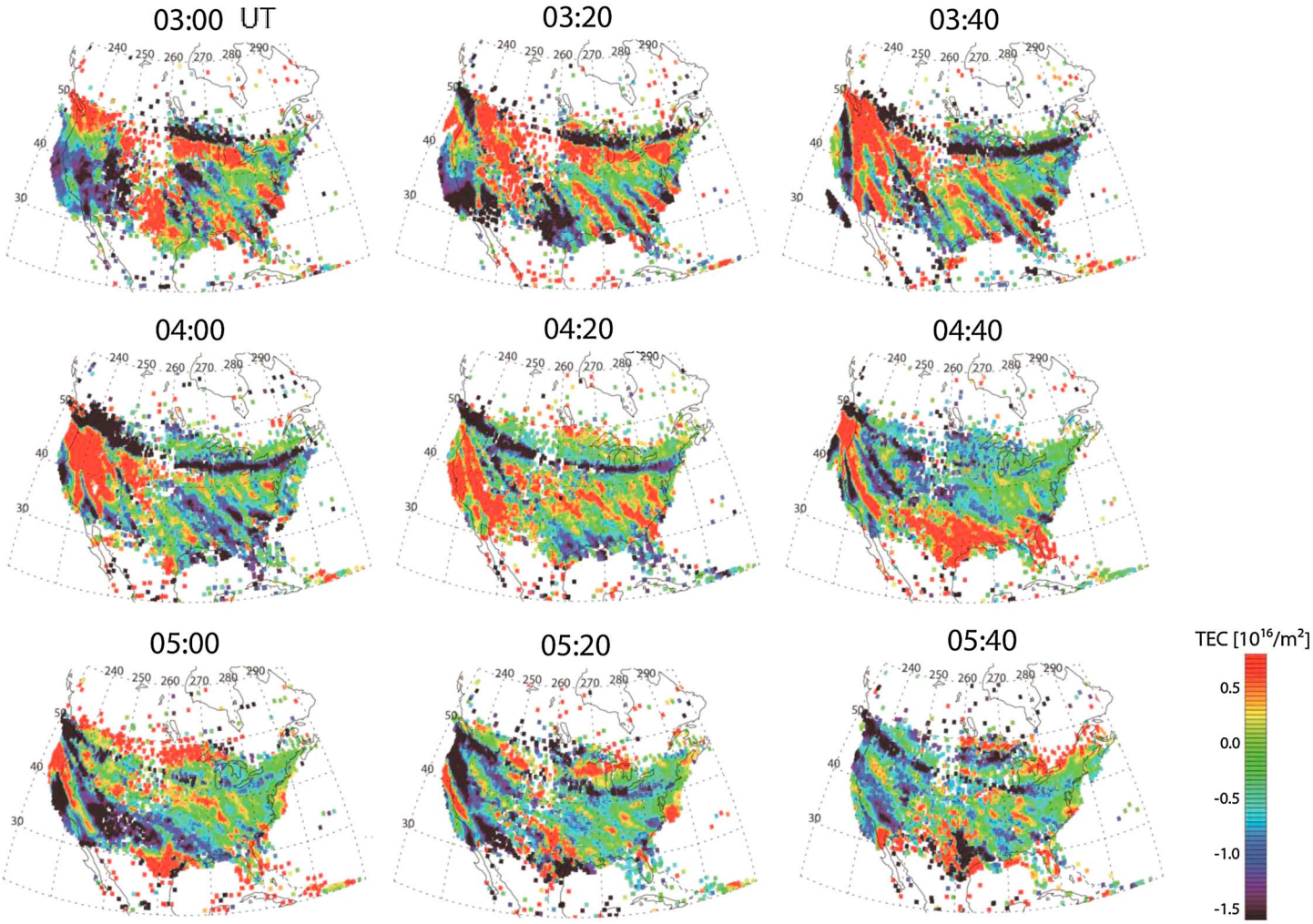


**Figure 4.** TEC perturbation maps in North America from 03:00 to 05:40 UT on 1 June 2013. Each map was produced with 30 s data.

Besides the uncertainties in the tilt direction and zonal motion of bubbles in middle latitudes, we did not find abnormalities in the bubbles detected on that night. In Figure 2b, the plasma density at the locations of bubbles is ~$10^4$ $cm^{-3}$ and the longitudinal width of bubbles is a few degrees. These are the characteristics of typical bubbles. When CINDI detected bubbles in the equatorial region (4.0 UT), the all-sky imager had already detected emission depletions at the magnetic latitude of 35°N. If the emission depletions at the magnetic latitude of 35°N (~3500 km in altitude) were produced by growing bubbles, we would expect the plasma density drop of ~$10^3$ $cm^{-3}$ at the locations of bubbles because of a severe uplift [e.g., *Kil and Lee*, 2013]. But the severe density drop did not appear. The emission depletions in the all-sky images extended to higher latitudes as time progressed. *Martinis et al.* [2015] explained the latitudinal extension of the emission depletions by the growth of bubbles. Comparing the observations in Figures 2b and 2c, bubbles appear to decay rather than grow with time. In the longitude of 240°–270° (bubbles in this longitude interval have the potential to be the source of the emission depletions in the all-sky images), the depletion depths and widths of the bubbles in earlier orbit (Figure 2b) are greater than those in later orbit (Figure 2c). One bubble near 250°E is an exception and can be interpreted to be the source of one of the emission depletions in the all-sky images. However, more than one emission depletion appears in the all-sky images.

## 4. The Role of MSTIDs

In the all-sky images shown in Figure 1, the emission depletions are aligned in the northwest-southeast direction and move from northeast to southwest. These properties are often observed from nighttime MSTIDs in TEC

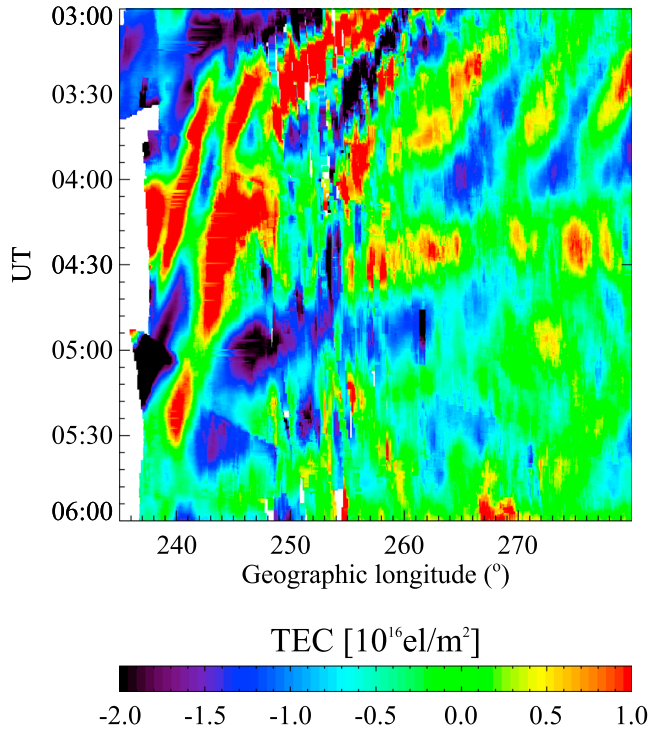


**Figure 5.** The keogram produced using the TEC perturbation data at 35°N geographic latitudes between 03:00 and 06:00 UT on 1 June 2013.

maps and airglow images [e.g., *Miller et al.*, 2014; *Saito et al.*, 2001; *Tsugawa et al.*, 2007]. To show the MSTID activity in North America on 1 June 2013, Figure 4 presents the TEC perturbation maps from 03:00 to 05:40 UT. The data points are sparse over Mexico because each TEC fluctuation map was produced with 30 s data. The ionospheric structures are tilted in the northwest-southeast direction and appear to move southwestward. The TEC map at 05:20 UT shows the ionospheric disturbance 1 min after the observation of the all-sky image in Figure 3a. The TEC perturbation maps demonstrate the existence of ionospheric disturbances in broad longitudes and latitudes in North America on the night of June 1.

To investigate the zonal movement of the TEC perturbation, a keogram was produced using the TEC perturbation data at 35°N geographic latitudes between 03:00 and 06:00 UT on 1 June. The keogram produced with the TEC perturbation maps of 30 s resolution is shown in Figure 5. Westward propagating wave features are visible at 03:00–04:00 LT in the longitude of 255°–280°E. The wavelength (~7°) and phase velocity (~190 m $s^{-1}$) of the wave features are within typical ranges of MSTIDs. Wave features are difficult to identify at later hours. However, the keogram shows the westward movement of ionospheric structures in the longitude of 245°–255°E around the time (05:19 UT) of the all-sky image in Figure 3a. The westward velocity (~40 m $s^{-1}$) of the ionospheric structures after 04:00 UT is much smaller than that before 04:00 UT.

## 5. Discussion

MSTIDs were active in North America and bubbles were detected in the equatorial region. Therefore, either of them can be considered to be the source of the emission depletions over Mexico. The source of the emission depletions is difficult to assess with direct evidence because the critical observation that supports the MSTID activity over Mexico is absent and the plasma depletions at intermediate latitudes that are critical for the verification of the connection of equatorial bubbles to middle-latitude emission depletions are also absent. We discuss the validity of the two hypotheses by comparing their weaknesses and strengths.

The strengths of the MSTID hypothesis over the bubble hypothesis are the westward motion and westward tilt of the middle-latitude emission depletions. The westward tilt of the MSTID features in North America is evident in the TEC perturbation maps. The emission depletions in all-sky images show the westward movement of about 1° per hour (~30 m $s^{-1}$). This velocity does not significantly deviate from the velocity (~40 m $s^{-1}$) of the ionospheric structures (TEC perturbations) at 35°N after 04:00 UT. However, we cannot verify how well the velocity at 35°N represents the velocity at 25°N (Mexico). The strengths of the MSTID hypothesis are the major weaknesses of the bubble hypothesis. As described in section 3, the westward motion of the westward tilted (with respect to geographic meridian) emission depletions is difficult to explain by the eastward motion of the eastward titled (with respect to geographic meridian) bubbles.

The strength of the bubble hypothesis is the observation of the emergence of the emission depletions from the south. The widths of the emission depletions (~300 km) are also consistent with the bubble size. If the

all-sky images reveal both the weakness and strength of the bubble hypothesis, which factor is more critical in the assessment of the validity of the bubble hypothesis? If bubbles are not the source of the emission depletions, can we satisfactorily explain the properties of the emission depletions with MSTIDs?

The apparent emergence of the emission depletions from the south instead of the appearance of them in the whole field of view can be the weakness of the MSTID hypothesis. This was the major reason that *Martinis et al*. [2015] did not interpret the emission depletions as MSTIDs. We used the expression "apparent emergence" because the interpretation of optical images is not straightforward. The appearance of ionospheric structures in optical images is affected by the background ionospheric conditions, severity of plasma depletion, and weather (clouds). The MSTID features were identified in the southwestern states (New Mexico, Arizona, and Texas) of the United States by the TEC perturbation maps, but those features were not clearly visible in the airglow images. Therefore, lack of the MSTID signature in the airglow images is related to the sensitivity of the imager. If the plasma depletion in MSTIDs was severer and the background plasma density was higher at lower latitudes, the all-sky imager would preferentially detect MSTIDs in the south of the field of view. *Martinis et al*. [2015] ignored MSTIDs, but arguably, the MSTID signature exists in their airglow images. In Figure 1, the structures in the northwest-southeast direction can be found in any image. They look like MSTIDs. The red dotted lines in the image at 03:42 UT provide guidelines of some emission depletion bands. The intense emission depletions observed in the south of the field of view are aligned with the emission depletion bands indicated with the red dotted lines. In the images at 05:21–06:34 UT in Figure 1, the intense emission depletions in the south appear to extend to the north. We think that this phenomenon is related to the brightness of the background rather than the growth of bubbles. The preexisting MSTID features seemed to appear as the background became brighter.

*Nishioka et al*. [2009] reported the development of super-MSTIDs over Japan during the geomagnetic storm of 10 November 2004 (minimum $Dst = -263$ nT). The ionospheric perturbations on that night were called super-MSTIDs because the perturbations showed the MSTID characteristics (northwest-southeast direction wavefront and its apparent movement from northeast to southwest), and the amplitude of the perturbations was about 10 times greater than that of normal MSTIDs. The TEC depletions at the troughs of the super-MSTIDs were more than 10 TECU (total electron content unit, 1 TECU = $10^{16}$ el $m^{-2}$). Those TEC depletions were not interpreted as bubbles because they showed the MSTID characteristics described above. We emphasize that severe plasma depletions or emission depletions can be produced in association with MSTIDs. The emission depletions produced by bubbles and MSTIDs are not distinguishable by simply examining their morphology or intensity [e.g., *Miller et al*., 2009].

## 6. Conclusions

We have investigated the source of the OI 630.0 nm emission depletions observed over Mexico on 1 June 2013. Those middle-latitude emission depletions were interpreted as equatorial plasma bubbles [*Martinis et al*., 2015]. Our study pointed out two uncertainties (zonal motion and tilt direction) in the interpretation of the middle-latitude emission depletions. First, the middle-latitude emission depletions showed westward drift, but the equatorial ionosphere showed eastward drift. We could not identify whether the reversal of the zonal plasma motion had occurred at middle latitudes. Second, the middle-latitude emission depletions were tilted westward, whereas equatorial bubbles showed eastward tilt with respect to the geographic meridian. We could not identify whether the tilt of bubbles had turned westward at higher latitudes. The middle-latitude emission depletions showed the latitudinal extension (growth) during the period of 03:42–06:34 UT. However, the CINDI observations at 03:50–05:50 UT did not provide convincing evidence for the growth of bubbles when the emission depletions grew. Because intense MSTIDs occurred over the United States on that night and their characteristics were consistent with those of the middle-latitude emission depletions, the emission depletions over Mexico could be interpreted in terms of MSTIDs.

**Acknowledgments**

This work was supported by Korea Polar Research Institute (PE16090), Wright-Patterson Air Force Base, Stuart S. Janney Publication Program in JHU/APL, and National Science Foundation aeronomy program (AGS-1237276). E.S. Miller acknowledges support from National Science Foundation grant AGS-1463967. Y.-S. Kwak acknowledges the "Planetary system research for space exploration" project and basic research funding from the Korea Astronomy and Space Science Institute (KASI). The GPS data used in this study were provided via the ftp servers of CORS, SOPAC, IGS, and UNAVCO. The GPS data collection and processing were performed with the Science Cloud at National Institute of Information Communications Technology in Tokyo, Japan. The SSUSI, TEC, and CINDI data are available by contacting H. Kil (hyosub.kil@jhuapl.edu). The OI 630 nm images taken at the McDonald Observatory were adopted from *Martinis et al*. [2015].

## References

Fejer, B. G., E. R. de Paula, S. A. González, and R. F. Woodman (1991), Average vertical and zonal *F* region plasma drifts over Jicamarca, *J. Geophys. Res.*, *96*, 13,901–13,906, doi:10.1029/91JA01171.

Fritts, D. C., and M. J. Alexander (2003), Gravity wave dynamics and effects in the middle atmosphere, *Rev. Geophys.*, *41*(1), 1003, doi:10.1029/2001RG000106.

Heelis, R. A., W. R. Coley, A. G. Burrell, M. R. Hairston, G. D. Earle, M. D. Perdue, R. A. Power, L. L. Harmon, B. J. Holt, and C. R. Lippincott (2009), Behavior of the $O^+/H^+$ transition height during the extreme solar minimum of 2008, *Geophys. Res. Lett.*, *36*, L00C03, doi:10.1029/2009GL038652.

Huba, J. D., G. Joyce, and J. Krall (2008), Three dimensional equatorial spread *F* modeling, *Geophys. Res. Lett.*, *35*, L10102, doi:10.1029/2008GL033509.

Hunsucker, R. D. (1982), Atmospheric gravity waves generated in the high-latitude ionosphere: A review, *Rev. Geophys.*, *20*, 293–315, doi:10.1029/RG020i002p00293.

Kelley, M. C. (1989), *The Earth's Ionosphere*, Academic Press, San Diego, Calif.

Kil, H., and R. A. Heelis (1998), Global distribution of density irregularities in the equatorial ionosphere, *J. Geophys. Res.*, *103*(A1), 407–417, doi:10.1029/97JA02698.

Kil, H., and W. K. Lee (2013), Are plasma bubbles a prerequisite for the formation of broad plasma depletions in the equatorial *F* region?, *Geophys. Res. Lett.*, *40*, 3491–3495, doi:10.1002/grl.50693.

Kil, H., S.-Y. Su, L. J. Paxton, B. C. Wolven, Y. Zhang, D. Morrison, and H. C. Yeh (2004), Coincident equatorial bubble detection by TIMED/GUVI and ROCSAT-1, *Geophys. Res. Lett.*, *31*, L03809, doi:10.1029/2003GL018696.

Kil, H., R. A. Heelis, L. J. Paxton, and S.-J. Oh (2009), Formation of a plasma depletion shell in the equatorial ionosphere, *J. Geophys. Res.*, *114*, A11302, doi:10.1029/2009JA014369.

Kil, H., W. K. Lee, Y.-S. Kwak, Y. Zhang, L. J. Paxton, and M. Milla (2014), The zonal motion of equatorial plasma bubbles relative to the background ionosphere, *J. Geophys. Res. Space Physics*, *119*, 5943–5950, doi:10.1002/2014JA019963.

Makela, J. J., and E. S. Miller (2008), Optical observations of the growth and day-to-day variability of equatorial plasma bubbles, *J. Geophys. Res.*, *113*, A03307, doi:10.1029/2007JA012661.

Martinis, C., and M. Mendillo (2007), Equatorial spread *F*-related airglow depletions at Arecibo and conjugate observations, *J. Geophys. Res.*, *112*, A10310, doi:10.1029/2007JA012403.

Martinis, C., J. Baumgardner, M. Mendillo, J. Wroten, A. Coster, and L. Paxton (2015), The night when the auroral and equatorial ionospheres converged, *J. Geophys. Res. Space Physics*, *120*, 8085–8095, doi:10.1002/2015JA021555.

Miller, E. S., J. J. Makela, and M. C. Kelley (2009), Seeding of equatorial plasma depletions by polarization electric fields from middle latitudes: Experimental evidence, *Geophys. Res. Lett.*, *36*, L18105, doi:10.1029/2009GL039695.

Miller, E. S., H. Kil, J. J. Makela, R. A. Heelis, E. R. Talaat, and A. Groves (2014), Topside signature of medium-scale traveling ionospheric disturbances, *Ann. Geophys.*, *32*, 959–965, doi:10.5194/angeo-32-959-2014.

Nishioka, M., A. Saito, and T. Tsugawa (2009), Super-medium-scale traveling ionospheric disturbance observed at midlatitude during the geomagnetic storm on 10 November 2004, *J. Geophys. Res.*, *114*, A07310, doi:10.1029/2008JA013581.

Otsuka, Y., K. Shiokawa, T. Ogawa, and P. Wilkinson (2004), Geomagnetic conjugate observations of medium-scale traveling ionospheric disturbances at midlatitude using all-sky airglow imagers, *Geophys. Res. Lett.*, *31*, L15803, doi:10.1029/2004GL020262.

Paxton, L. J., D. Morrison, Y. Zhang, H. Kil, B. Wolven, B. S. Ogorzalek, D. C. Humm, and C.-I. Meng (2002), Validation of remote sensing products produced by the Special Sensor Ultraviolet Scanning Imager (SSUSI): A far UV imaging spectrograph on DMSP F-16 SPIE Optical Spectroscopic Techniques and Instrumentation for Atmospheric and Space Research IV, vol. 4485, 338–348.

Saito, A., et al. (2001), Traveling ionospheric disturbances detected in FRONT campaign, *Geophys. Res. Lett.*, *28*(4), 689–692, doi:10.1029/2000GL011884.

Shiokawa, K., C. Ihara, Y. Otsuka, and T. Ogawa (2003), Statistical study of nighttime medium-scale traveling ionospheric disturbances using midlatitude airglow images, *J. Geophys. Res.*, *108*(A1), 1052, doi:10.1029/2002JA009491.

Shiokawa, K., Y. Otsuka, T. Ogawa, and P. Wilkinson (2004), Time evolution of high-altitude plasma bubbles imaged at geomagnetic conjugate points, *Ann. Geophys.*, *22*, 3137–3143, doi:10.5194/angeo-22-3137-2004.

Shiokawa, K., Y. Otsuka, N. Nishitani, T. Ogawa, T. Tsugawa, T. Maruyama, S. E. Smirnov, V. V. Bychkov, and B. M. Shevtsov (2008), Northeastward motion of nighttime medium-scale traveling ionospheric disturbances at middle latitudes observed by an airglow imager, *J. Geophys. Res.*, *113*, A12312, doi:10.1029/2008JA013417.

Tsugawa, T., Y. Otsuka, A. J. Coster, and A. Saito (2007), Medium-scale traveling ionospheric disturbances detected with dense and wide TEC maps over North America, *Geophys. Res. Lett.*, *34*, L22101, doi:10.1029/2007GL031663.

Vadas, S. L., and G. Crowley (2010), Sources of the traveling ionospheric disturbances observed by the ionospheric TIDDBIT sounder near Wallops Island on 30 October 2007, *J. Geophys. Res.*, *115*, A07324, doi:10.1029/2009JA015053.

Vadas, S. L., and H. Liu (2009), Generation of large-scale gravity waves and neutral winds in the thermosphere from the dissipation of convectively generated gravity waves, *J. Geophys. Res.*, *114*, A10310, doi:10.1029/2009JA014108.